BMC Plant Biology

RESEARCH

Open Access

Phylogenomics and adaptive evolution of hydrophytic umbellifers (tribe Oenantheae, Apioideae) revealed from chloroplast genomes

Jun Wen[1], Jun-Wen Zhu[1], Xu-Dong Ma[1], Hui-Min Li[1], Bao-Cheng Wu[1], Wei Zhou[1], Jia-Xin Yang[2] and Chun-Feng Song[1*]

Abstract

Background Tribe Oenantheae consists mainly of aquatic species within the Apioideae. The unique morphology and habitat distinguish this group from other Apioideae groups. However, the genomic information of these group species has not been widely developed, and the molecular mechanisms of adaptive evolution remain unclear.

Results We provide comparative analyses on 30 chloroplast genomes of this tribe representing five genera to explore the molecular variation response to plant adaptations. The Oenantheae chloroplast genomes presented typical quadripartite structures, with sizes ranging from 153,024 bp to 155,006 bp. Gene content and order were highly conserved with no significant expansion or contraction observed. Seven regions (*rps16* intron–*trnK*, *rpoB*–*trnC*, *trnE*–*trnT*–*psbD*, *petA*–*psbJ*, *ndhF*–*rpl32*–*trnL*, *ycf1a*–*rps15*, and *ycf1a* gene) were identified as remarkable candidate DNA markers for future studies on species identification, biogeography, and phylogeny of tribe Oenantheae. Our study elucidated the relationships among the genera of tribe Oenantheae and subdivided the genera of *Sium* and *Oenanthe*. However, relationships among the *Oenanthe* I clade remain to be further clarified. Eight positively selected genes (*accD*, *rbcL*, *rps8*, *ycf1a*, *ycf1b*, *ycf2*, *ndhF*, and *ndhK*) were persuasively detected under *site* models tests, and these genes might have played roles in Oenantheae species adaptation to the aquatic environments.

Conclusions Our results provide sufficient molecular markers for the subsequent molecular studies of the tribe Oenantheae, and promote the understanding of the adaptation of the Oenantheae species to aquatic environments.

Keywords Oenantheae, Adaptation, Phylogeny, Positive selection, Candidate DNA markers

Background

Oenantheae Dumort is a special tribe of Apioideae (Apiaceae) that is morphologically and ecologically well-defined. Species of this tribe are generally aquatic with clumped fibrous or tuberous-thickened roots (usually rooted at the base of the stem), and pericarp of the fruits with varying degrees of corky-thickened. Molecular phylogenetic studies in recent years have shown that Oenantheae is currently recognized as a natural and stable major clade of Apioideae, located in the middle of the phylogenetic tree [1–7]. Pollen of Oenantheae species vary in shape, covering almost every type from

*Correspondence:
Chun-Feng Song
cfsong79@cnbg.net
[1] Jiangsu Key Laboratory for the Research and Utilization of Plant Resources, Institute of Botany, Jiangsu Province and Chinese Academy of Sciences (Nanjing Botanical Garden Mem. Sun Yat-Sen), Nanjing 210014, China
[2] School of Life Science and Food Engineering, Huaiyin Institute of Technology, Huai'an 223000, China

primitive to evolutionary [8, 9]. The integration of multiple traits (morphological, phylogenetic, ecological, and palynological) has shown that Oenantheae is the key group in studying the evolutionary history of Apioideae. The tribe currently contains about 24 genera and 120 species: including 5 genera (*Berula* W. D. J. Koch, *Cicuta* L., *Cryptotaenia* DC., *Oenanthe* L., and *Sium* L.) distributed in both Eurasia and North America; 12 genera (*Atrema* DC., *Ptilimnium* Raf., *Tiedemannia* DC., *Harperella* Rose, *Limnosciadium* Mathias & Constance, *Cynosciadium* DC., *Lilaeopsis* Greene, *Neogoezia* Hemsl., *Trepocarpus* Nutt. ex DC., *Daucosma* Engelm. & A.Gray, *Oxypolis* Raf., and *Perideridia* Rchb.) [10–12] endemic to North America; 3 genera [*Caropsis* (Rouy & E.G.Camus) Rauschert、*Lereschia* Boiss., and *Trocdaris* Raf.] [5, 12] and one hybrid genus (× *Beruladium* A.C.Leslie) [13] endemic to Europe; one genus (*Helosciadium* W.D.J.Koch) [14] distributed in both Eurasia and Africa; one monotypic genus (*Apodicarpum* Makino) [3] endemic to Asia; and one species (*Peucedanum sandwicense* Hillebr.) [12] endemic to Hawaii. There are 5 genera and around 17 species distributed in China [15].

Previous studies have shown that Oenantheae was recognized as a monophyletic tribe of Apioideae, but the relationships among the genera within this tribe have not been completely resolved. Most of the previous studies on the phylogeny of Oenantheae were carried out based on small molecular markers, including nrDNA ITS [5, 10–12, 16–19], *rps16* intron [20], *trnQ–trnK* [18], *psbI–*$^{5'}$*trnK*$^{(UUU)}$ [11], and *rps16–*$^{5'}$*trn*K$^{(UUU)}$ [12, 14]. The intergeneric relationships of most genera within Oenantheae have been clarified, except for the genera within the *Sium* alliance. Recently, a biogeographical study on Oenantheae was implemented under comprehensive sampling using ITS and *rps16–trnK* markers [12]. The phylogenetic reconstruction results showed that Oenantheae was well divided into four lineages and two individual species, including the North American (NA) endemic clade [10, 19], the *Cicuta* & *Oenanthe* group [21], the *Sium* alliance [14], the *Perideridia* clade [22], *Caropsis verticillatoinundata* (Thore) Rauschert, and *Trocdaris verticillatum* (L.) Raf [12]. The relationships among genera within the North American (NA) endemic clade and the *Cicuta* & *Oenanthe* group were highly supported, but that of the *Sium* alliance (which was formerly known as Old World endemics clade in Spalik et al., 2009) were still controversial. The relationships among genera within the *Sium* alliance were poorly supported. Mostly, the insufficient informative sites of small molecular markers were suggested to be the main reason for the depressed resolution of phylogenies [2, 6].

Chloroplast genomes have been widely used for the reconstruction of plant phylogenies in recent years [6, 23–28]. Compared with small molecular markers, chloroplast genomes have sufficient information sites to meet the needs of phylogenetic reconstruction. The unique mode of inheritance ultimately reflected the "true" phylogenetic relationships of a given lineage. Nearly 2.2% of the published chloroplast genomes (NCBI, September 2023) were generated from Apiales species [27], most of which were from Apiaceae species. Apiaceae chloroplast genomes generally shared a typical quadripartite structure including a larger single copy region (LSC), a small single copy region (SSC), and two inverted repeat regions (IRA and IRB). However, the characteristics of genome structure varied among different species/genera of Apiaceae [6, 29, 30]. Comparative genomic studies concerning the characteristics of genes or functional groups of genes are of great importance in understanding plastome evolution and phylogenetic inference [27, 29, 31–33]. The chloroplast genome data were successfully used for phylogenetic reconstruction of Apiaceae in many studies [6, 24, 29, 30, 34–37]. However, the chloroplast genome of Oenantheae has not been paid much attention, and most of the chloroplast genome studies on this tribe involved individual species [38–41] or specific genus (for genus *Sium*) [42]. Regrettably, there was a lack of plastid phylogenomic analysis conducted for this tribe, and the genome differences of intergeneric plastids are still unknown within Oenantheae.

In this study, we filled this gap with a comparative analysis of the chloroplast genomes of 30 taxa (covering five genera) within Oenantheae. We conducted comprehensive analyses (1) to reveal the chloroplast genome characteristics and evolution of Oenantheae; (2) to identify suitable hotspot regions to use as candidate DNA barcodes for genera identification within the tribe; (3) to investigate the efficacy of chloroplast genome in resolving the relationships within the tribe. This is the first comprehensive chloroplast genome analysis of the tribe Oenantheae, which will provide genetic resources and complete the phylogeny analysis of this tribe. This study is crucial for reconstructing the phylogeny and evolution of the global Oenantheae.

Materials and methods

Taxon sampling, DNA extraction, genome sequencing, assembly, and annotation

Seventeen chloroplast genomes were newly sequenced, covering 4 genera and eleven species within Oenantheae (Fig. 1). The collections and voucher information for these newly sequenced species are provided in Table S1. Fresh and well-developed leaves were collected and dried in silica gel. Total genomic DNA was extracted from the leaf tissues using the Plant Genomic DNA Kit following the manufacturer's protocol (Tiangen Biotech, Beijing,

Fig. 1 Morphological diversity of Oenantheae species. **A**, *Oenanthe javanica*; **B**, *O. hookeri*; **C**, *O. thomsonii*; **D**, *Sium ventricosum*; **E**, *S. serra*; **F**, *S. suave*; **G**, *Cicuta virosa*; **H**, *Cryptotaenia canadensis*; **I**, *Cryptotaenia japonica*

China), and the DNA quality and purity were further determined with the agarose gel electrophoresis. The high-quality DNA was used for library construction and sequencing. Paired-end sequencing libraries were generated on the Illumina Novaseq 6000 platform at Novogene (Beijing, China), with 2×150 bp paired-end reads and an insert size of 300 bp. DNA libraries were prepared using Rapid Plus DNA Lib Prep Kit for Illumina (RK20208). We sequenced 3G raw data for each sample.

Qualities of raw reads were checked by FastQC v0.11.9 [43]. The chloroplast genomes were assembled using NOVOPlasty v4.3.3 [44]. The Rubisco-bis-phosphate oxygenase (RUBP) sequences from multiple reference genomes (Table 1) were extracted to serve as seed files for different genera as appropriate. The assembled sequences were checked and annotated under Geneious Prime 2023.2.1 (created by the Biomatters development team, Ltd.), with gaps or degenerate bases corrected by Sanger sequencing. The chloroplast genome maps were drawn using OGDRAW [45]. All newly generated chloroplast genomes have been uploaded to the National Center for Biotechnology Information (NCBI) and are accompanied by detailed accession numbers, as shown in Table 1.

Chloroplast genomes comparative analyses

A total of 30 chloroplast genomes from five genera of Oenantheae have been adopted to implement comparative analyses. Detailed accession numbers are listed in Table 1. We investigated the chloroplast genome structure of Oenantheae taxa, including gene number, length, and GC content of the whole genomes. Boundaries of the large single copy (LSC), small single copy (SSC), and inverted repeat (IR) regions among Oenantheae chloroplast genomes were compared in Geneious Prime 2023.2.1 to detect the IR expansion/contraction. To identify potential rearrangement and inversion events in chloroplast genomes, we utilized the Mauve Alignment [46] implemented in Geneious Prime.

To identify mutation hotspot regions among species within Oenantheae, the whole chloroplast genomes aligned matrix generated from MAFFT v7 [47] plug-in Geneious Prime 2023.2.1 was used to calculate nucleotide

Table 1 Summary of major characteristics of the Oenantheae chloroplast genomes, including sequence size (bp), number of genes, GC content, GenBank accession number, and Vouchers/References

Taxon	Size (bp)				GC content				Number of Genes					GenBank accession No.	Vouchers/References
	Total	LSC	IRs	SSC	Total	LSC	IR	SSC	Total	CDS	rRNA	tRNA	pseudogene		
Cicuta virosa	**154,438**	**84,193**	**26,355**	**17,535**	**37.50%**	**35.60%**	**42.70%**	**30.80%**	**133**	**86**	**8**	**37**	**2**	**PQ283862**	**LHM1252**
Cicuta virosa	154,569	84,177	26,407	17,578	37.50%	35.60%	42.70%	31.00%	133	86	8	37	2	NC_037711	NCBI direct submission
Cicuta virosa	**154,341**	**84,066**	**26,377**	**17,521**	**37.50%**	**35.60%**	**42.70%**	**30.90%**	**133**	**86**	**8**	**37**	**2**	**PQ283863**	**WJ2368**
Oenanthe hookeri	**154,597**	**84,414**	**26,456**	**17,271**	**37.50%**	**35.60%**	**42.70%**	**31.10%**	**133**	**86**	**8**	**37**	**2**	**PQ283867**	**WJ2334**
Oenanthe javanica	154,246	84,096	26,456	17,238	37.60%	35.80%	42.70%	31.30%	133	86	8	37	2	NC_049874	Zhang et al., 2020b [41]
Oenanthe javanica	**154,378**	**84,118**	**26,491**	**17,278**	**37.60%**	**35.80%**	**42.70%**	**31.20%**	**133**	**86**	**8**	**37**	**2**	**PQ283868**	**WJ2305_02**
Oenanthe javanica	**154,048**	**84,063**	**26,244**	**17,497**	**37.60%**	**35.80%**	**42.80%**	**31.30%**	**133**	**86**	**8**	**37**	**2**	**PQ283869**	**WJ2320**
Oenanthe javanica	**154,223**	**84,073**	**26,456**	**17,238**	**37.60%**	**35.80%**	**42.70%**	**31.20%**	**133**	**86**	**8**	**37**	**2**	**PQ283870**	**WJ2372_AH01**
Oenanthe linearis	**154,486**	**84,286**	**26,458**	**17,284**	**37.50%**	**35.60%**	**42.70%**	**31.10%**	**133**	**86**	**8**	**37**	**2**	**PQ283871**	**ZJW034**
Oenanthe linearis*subsp.*rivulari	**154,628**	**84,348**	**26,451**	**17,378**	**37.50%**	**35.60%**	**42.70%**	**31.00%**	**133**	**86**	**8**	**37**	**2**	**PQ283872**	**NZD2301**
Oenanthe linearis*subsp.*rivulari	**154,660**	**84,426**	**26,451**	**17,332**	**37.50%**	**35.60%**	**42.70%**	**31.10%**	**133**	**86**	**8**	**37**	**2**	**PQ283873**	**WJ2319**
Oenanthe thomsonii	**154,640**	**84,373**	**26,479**	**17,309**	**37.50%**	**35.60%**	**42.70%**	**31.10%**	**133**	**86**	**8**	**37**	**2**	**PQ283875**	**WJ2321**
Oenanthe virgata	154,464	84,410	26,445	17,163	37.50%	35.60%	42.70%	31.20%	133	86	8	37	2	KX832335	Spooner et al., 2017 [39]
Oenanthe pimpinelloides	**154,438**	**84,415**	**26,421**	**17,181**	**37.60%**	**35.70%**	**42.70%**	**31.30%**	**133**	**86**	**8**	**37**	**2**	**PQ283874**	**wj20230607_01**
Cryptotaenia canadensis	**154,101**	**84,048**	**26,435**	**17,183**	**37.50%**	**35.50%**	**42.70%**	**30.90%**	**133**	**86**	**8**	**37**	**2**	**PQ283864**	**WJ220908**
Cryptotaenia japonica	**153,385**	**83,616**	**26,419**	**16,931**	**37.50%**	**35.60%**	**42.70%**	**30.90%**	**133**	**86**	**8**	**37**	**2**	**PQ283865**	**WJ2375**
Cryptotaenia japonica	**153,228**	**83,451**	**26,417**	**16,943**	**37.50%**	**35.60%**	**42.70%**	**30.90%**	**133**	**86**	**8**	**37**	**2**	**PQ283866**	**WJ2384**
Cryptotaenia japonica	153,259	83,477	26,419	16,944	37.50%	35.60%	42.70%	30.90%	133	86	8	37	2	NC_046737	Luo and Yu, 2019 [40]
Sium crispulifolium	154,099	84,707	26,150	17,092	37.40%	35.40%	42.70%	31.00%	133	86	8	37	2	OP234518	Zhou et al., 2023 [42]
Sium medium	154,598	84,116	26,472	17,538	37.40%	35.50%	42.70%	30.70%	133	86	8	37	2	NC_072108	Zhou et al., 2023 [42]
Sium ninsi	155,006	85,036	26,208	17,554	37.40%	35.50%	42.70%	30.60%	133	86	8	37	2	NC_072107	Zhou et al., 2023 [42]
Sium serra	**154,690**	**84,491**	**26,223**	**17,753**	**37.40%**	**35.60%**	**42.70%**	**30.60%**	**133**	**86**	**8**	**37**	**2**	**PQ283876**	**WJ2374**
Sium suave	154,676	84,155	26,469	17,583	37.40%	35.50%	42.70%	30.70%	133	86	8	37	2	NC_071929	Zhou et al., 2023 [42]
Sium suave	154,642	84,111	26,466	17,599	37.40%	35.50%	42.70%	30.70%	133	86	8	37	2	OP234519	Zhou et al., 2023 [42]
Sium suave	**154,646**	**84,128**	**26,466**	**17,586**	**37.40%**	**35.50%**	**42.70%**	**30.70%**	**133**	**86**	**8**	**37**	**2**	**PQ283877**	**WBC2301**
Sium tenue	154,929	84,952	26,204	17,569	37.40%	35.50%	42.70%	30.70%	133	86	8	37	2	NC_072106	Zhou et al., 2023 [42]
Sium ventricosum	153,024	84,294	24,970	18,790	37.40%	35.50%	43.10%	30.80%	133	86	8	37	2	NC_070095	NCBI direct submission
Sium ventricosum	153,029	84,300	24,970	18,789	37.40%	35.50%	43.10%	30.80%	133	86	8	37	2	OP234514	Zhou et al., 2023 [42]
Sium ventricosum	**153,031**	**84,273**	**25,027**	**18,704**	**37.40%**	**35.50%**	**43.10%**	**30.80%**	**133**	**86**	**8**	**37**	**2**	**PQ283878**	**WJ2339**
Tiedemannia filiformis subsp. greenmannii	154,737	84,581	26,510	17,136	37.30%	35.40%	42.60%	30.40%	133	86	8	37	2	HM596071	Downie and Jansen, 2015 [38]

diversity (Pi). The sliding window analysis was conducted using DnaSP v6.10 [48], with a step size of 200 bp and a window length of 600 bp. We performed additional nucleotide diversity calculations for specific regions, including fragments previously utilized in the phylogenetic analysis of Oenantheae, the protein-coding genes (PCGs), their coding sequences (CDSs), and introns.

Positively selected analyses

To understand the process of evolution of chloroplast protein-coding genes, we calculated the non-synonymous (Ka) and synonymous mutations (Ks) of the CDSs. The ratios between non-synonymous and synonymous mutations (ω = Ka/Ks) can reveal the direction and strength of nature selection acting on the protein. Values of $\omega < 1$, $= 1$, > 1 indicate negative purifying selection, neutral evolution, and positive selection, respectively [49]. A total of 80 CDSs were extracted from 30 chloroplast genomes of Oenantheae taxa, and the protein-coding sequence alignments were generated using *Translation Align* under the MAFFT program with stop codons removed accordingly. The *petN* and *psbN* genes were excluded due to their identical nucleotide sequences among taxa. Thus, only 78 CDSs were included in the later analysis. The DnaSP v6.10 was subsequently utilized to calculate the Ka and Ks.

We tested positive selection on site (codon) based models. Five (*petN*, *psbL*, *psbN*, *rps7*, and *ycf3*) were excluded from the testing due to having identical amino acid sequences. A total of 75 CDSs were employed to test positive selection. Firstly, 75 aligned CDSs were manually concatenated into a supermatrix in MEGA v7 [50] and subsequently used to infer an unrooted ML tree under RAxML v8.2.12 [51]. The unrooted ML tree and each CDS alignment served as input files in EasyCodeML analysis [52]. *Site* models in CodeML [53–55] executed in EasyCodeML were utilized to detect positively selected sites of PCGs in Oenantheae chloroplast genomes. These models treat the ω ratio for any site (codon) in the gene as a random variable from a statistical distribution, thus allowing ω to vary among codons [53, 54, 56]. Two pairs of particularly effective site models were adopted in our study: M1a (*Nearly Neutral*) vs. M2a (*Positive Selection*) and M7 (*beta*) vs. M8 (*beta&ω*). For these two tests, M1a and M7 are null models that do not allow for any sites with $\omega > 1$, and the M2a and M8 are alternative models that allow some sites with $\omega > 1$. These tests were widely used for positive selection [32, 57–62]. The presence of some sites at which $\omega > 1$ was used to define positive selection [56]. Likelihood ratio tests (LRTs) [54] were performed to compare the null models against the alternative models. The *P*-values were calculated to measure the significance level of positive selection. If the LRT favors M2a or M8 ($P < 0.05$), we will identify sites in the genes that are under positive selection [56]. The Bayesian Empirical Bayes (BEB) method [57] was adopted and performed for the identification. A gene with LRT $P < 0.05$ and positively selected sites was considered a positively selected gene.

Phylogenetic reconstruction

A total of 32 taxa were sampled for phylogenetic analysis, including five genera from Oenantheae and two species from Scandiceae (Apioideae) as outgroups. The outgroups [*Anthriscus sylvestris* (L.) Hoffm., and *Torilis scabra* (Thunb.) DC.] were selected according to Wen et al., 2021, the NCBI accession numbers were MT561042 and MT561029, respectively. The 30 Oenantheae taxa contain 11 taxa from each genus *Sium* and *Oenanthe*, four taxa from *Cryptotaenia* species, three taxa from *Cicuta*, and one taxon from *Tiedemannia*. The five genera cover three lineages of Oenantheae (except for the *Perideridia* clade): including the *sium* alliance (*Sium* and *Cryptotaenia*), *Cicuta* & *Oenanthe* group, and Nouth American endemics clade (*Tiedemannia*). Eight datasets were adopted for reconstructing the phylogenetic tree. Five intergenic regions, including three small fragments previously used [1), *psbI–trnK*, 2), *rps16–trnK*, and 3), *trnQ–trnK*] [11, 12, 14, 18], 4), the noncoding region of the total genome, and 5), one dataset concatenated nine introns extracted from the corresponding PCGs (excluded introns of the *rpl2* and *ndhB* genes due to the very small Pi). Two protein-coding sequences (CDSs) matrixes: 6), one dataset concatenated eight CDSs with high nucleotide diversity value, and 7), another concatenated 78 CDS from the whole genome. 8), The entire genome matrix was also used for analyses.

Two methods were employed to conduct phylogenetic analysis: maximum likelihood (ML) and Bayesian inference (BI). The ML analysis was performed by RAxML v8.2.4 [51], under the GTRGAMMA model as suggested in the manual. Rapid bootstrap analysis was implemented using 1000 bootstrap replicates to search for the best-scoring ML tree. MrBayes v3.2.7a [63] was employed to conduct the BI analysis under the best-fit model GTR + I + G recommended by jModelTest v2.1.4 [64]. Two independent Markov chain Monte Carlo (MCMC) runs were performed, each with three heated chains and one cold chain for 10,000,000 generations. The average standard deviation of split frequencies should approach zero, otherwise generations will be added to continue the analysis. Each run started with a random tree, sampling trees every 1000 generations, with the initial 25% discarded as burn-in. The bootstrap support (BS) and posterior probability (PP) were used to measure the supports of the phylogenetic tree implemented under ML

and BI methods, respectively. The final tree was viewed in FigTree v1.4 [65].

Results and discussion

Gene characteristic diversity in Oenantheae chloroplast genomes

Among the seventeen newly sequenced plastid genomes, seven species were first reported. The size of Oenantheae chloroplast genomes ranged from 153,024 bp [*Sium ventricosum* (H.Boissieu) Li S.Wang & M.F.Watson, NC_070095] to 155,006 bp (*Sium ninsi* L.) (Table 1). Chloroplast genomes of Oenantheae species shared a typical quadripartite structure, which was consistent with that of most other Apioideae species [6, 29, 30, 36, 42], possessing two copies of IR regions (IRA and IRB, 24,970–26,510 bp) separated by the LSC region (83,451–85,036 bp) and SSC region (16,931–18,790 bp). The total GC content ranged from 37.30 to 37.60% roughly comparable to that in some other chloroplast genomes of Apioideae distal clades species [6, 66–70]. The IR region held the highest GC content (42.6–43.1%) when compared to LSC (35.4–35.8%) and SSC (30.4–31.3%) (Table 1, Fig. S1). The North American endemics *Tiedemannia filiformis subsp. Greenmannii* (Mathias & Constance) Feist & S.R.Downie showed the lowest GC content among the 30 Oenantheae chloroplast genomes in all regions (the total genome, LSC, SSC, IR regions) (Table 1). For the remaining species, GC contents of the total genome, LSC, and SSC were highest in the *Oenanthe* species, and lowest in the *Sium* species. The GC contents of IR regions were basically the same among species except *S. ventricosum*, which possessed a unique extra high GC content of 43.1%. We hypothesized that it might be related to the high-altitude habitat of this species. We reviewed the chloroplast genomes of Apioideae species, the GC content of IR regions of some high-altitude plants (e.g. *Pleurospermum* s. l.) did have high GC values (42.7–45.4%) [24], while others (e.g. *Tongoloa* H. Wolff) did not (40.5–42.4%) [37]. Therefore, the higher GC content may be related to the more complex evolutionary history of this species, which needs to be further studied.

Each of the 30 chloroplast genomes contained 133 genes, consisting of 86 PCGs, eight rRNA genes, 37 tRNA genes, and two pseudogenes. A total of 19 genes have been detected duplicated, including seven protein-coding genes (*rpl2*, *rpl23*, *ycf2*, *ndhB*, *rps7*, *rps12*, and *ycf1*), four rRNA genes (*rrn4.5*, *rrn5*, *rrn16*, and *rrn23*), seven tRNA genes (*trnA-UGC*, *trnI-GAU*, *trnI-CAU*, *trnL-CAA*, *trnN-GUU*, *trnR-ACG*, and *trnV-GAC*), and the pseudogene *ycf15*. Fifteen genes were owning some introns: 11 genes (*atpF*, *ndhA*, *rpoC1*, *petB*, *petD*, *rpl16*, *rps16*, and two copies of *ndhB* and *rpl2*) contained one intron, four genes (*clpP*, *ycf3*, and two copies of *rps12*) contained two introns. No significant expansion or contraction has been detected in Oenantheae chloroplast genomes (Table S2), so did the rearrangement and inversion events (Fig. S2). Each of the LSC/IRA junctions (J_{LA}) and SSC/IRA junctions (J_{SA}) in the Oenantheae chloroplast genomes were at the same positions. The J_{LA} was located between the *rpl2* and *trnH-GUG* genes, and the J_{SA} was at the *ycf1a* gene (the copy of the *ycf1* gene was largely located in the IRA region). The junction of LSC/IRB (J_{LB}) was located at the *rps19* gene, except for *Cicuta virosa* L. (no. LHM1252, intergenic region of *rps19* and *rpl2*), which was consistent with that mentioned in Wen et al., 2021. The junction of SSC/IRB (J_{SB}) was located at the *ycf1b* gene (the copy of *the ycf1* gene was largely located in the IRB region) or the overlap region of *ycf1b* and *ndhF*.

Mutation hotspot regions among species of Oenantheae

Gene sequences with high nucleotide diversity (Pi) were suggested to be mutation hotspot regions. The sliding window analyses across the 30 Oenantheae chloroplast genomes showed that the Pi ranged from 0.0000 to 0.0663 (Fig. 2, Table S3). Overall, 188 sequences were owning Pi > 0.015. Among them 89 sequences with Pi > 0.02 (highlighted with red dots in Figs. 2), 22 sequences with Pi > 0.03, and six sequences with Pi > 0.04 (Table S3). The results showed that the sequences with Pi > 0.02 were all located in LSC and SSC, and sequences in IR regions generally had significantly lower Pi (Fig. 2). The sequences with high Pi were identified. Sequences with Pi > 0.02 were located at 30 regions, including *matK–psbA*, *rps16–matK*, *rps16* intron–*trnK*, *rps16* intron, *rps16* intron–*psbK*, *psbK–psbI*, *psbI–trnS–trnG*, *trnG–atpA*, *atpH–atpF* intron, *atpI–atpH*, *rpoB–trnC–petN*, *petN–psbM*, *trnD–trnY–trnE–trnT–psbD*, *ycf3–trnS–rps4*, *rps4–trnT–trnL*, *trnL–trnF–ndhJ*, *rbcL–accD*, *accD*, *petA–psbJ–psbL*, *psbE–petL*, *clpP* intron, *clpP* intron–*psbB*, *rpl16* intron, *rps3–rpl16* intron, *ndhF–rpl32–trnL–ccsA*, *ccsA–ndhD*, *ndhI–ndhG*, *ndhA* intron, *ycf1a–rps15–ndhH*, *ycf1a* gene. Among these regions, 14 were formerly used or identified to reconstruct the phylogeny of Apiaceae groups [2, 42, 71–77]. Our study provides more alternative molecular markers for the phylogenetic studies of Apiaceae groups (especially for Apioideae major clades). Sequences with 0.03 < Pi < 0.04 were identified at seven regions, including *ycf1a* gene, *trnE–trnT–psbD*, *ndhF–rpl32–trnL*, *rpoB–trnC*, *ycf1a–rps15*, *petA–psbJ*, and *rps16* intron–*trnK* regions. Among these regions, the *ycf1a* gene, *trnE–trnT–psbD*, *ndhF–rpl32–trnL* regions also contained the sequences with Pi above 0.04 (Table S3, Fig. 2). Sequences with Pi > 0.02 were mostly distributed in intergenic regions or introns of genes, with only three CDSs of the PCGs (*rpl32*, *rps16*,

and *ycf1a*) owning Pi > 0.02 (Table S3, S4). In addition to the three, there were a few PCGs (*accD*, *ccsA*, *matK*, *ndhF*, and *rps15*) with Pi greater than 0.015 in their CDS regions. The remaining PCGs possessed generally low Pi (Table S4, Fig. 3A).

We calculated the Pi of genes, introns, and coding sequences (CDS) of the 11 genes that had introns (except the *rps12* gene). Compared with the genes and coding regions, the introns each possessed a high Pi, except for the case of *rps16* and *ndhB*. The Pi of these two genes are displayed as CDS > Gene > Intron (Fig. 3B). Overall, introns of five genes (including *rpl16*, *ndhA*, *rps16*, *clpP*, and *petB*) possessed Pi > 0.015, among them *rpl16* (0.0227) and *ndhA* (0.0213) with Pi above 0.02 (Table S5). The Pi of the 11 CDSs were very low, except for the *rps16* CDS (0.0215). The *rps16* intron has been used to infer the phylogeny and evolution of Apiaceae, the subfamily, and their major clades for a long time [2, 71–75, 77]. Our study found that both the CDS and intron of the *rps16* gene possessed Pi > 0.015. The Pi of other three small fragments previously used (*psbI–trnK*, *rps16–trnK*, and *trnQ–trnK*) in phylogenetic analyses of the Oenantheae group [11, 12, 14, 18] were also calculated with values above 0.02 (Table S6). Based on previous studies, all these fragments (*rps16* intron, *psbI–trnK*, *rps16–trnK*, and *trnQ–trnK*) provided a certain resolution in the phylogenetic analysis of Oenantheae, but could not completely resolve all relationships within the tribe. Thus, we proposed that sequence regions with Pi greater than 0.03 (*ycf1a* gene, *trnE–trnT–psbD*, *ndhF–rpl32–trnL*, *rpoB–trnC*, *ycf1a–rps15*, *petA–psbJ*, and *rps16* intron–*trnK* regions) can be considered as candidate barcodes for the phylogenetic analyses. We extracted the seven regions with Pi > 0.03 and aligned. All sequences are free of alignment ambiguities. A comparison of the number of variable sites, parsimony-informative positions, and the percent of parsimony-informative across these regions and the four previously used fragments have revealed that regions with Pi > 0.03 were identified as candidate DNA markers (Table S6).

Phylogenetic relationships among Oenantheae species inferred from multiple datasets

The robust phylogenetic trees were reconstructed from eight concatenated matrices, which exhibited clear relationships among genera within the tribe Oenantheae (Figs. 4 and 5). Our phylogenetic results strongly supported (BS = 100, PP = 1.00) that Oenantheae was divided into three clades: the *Cicuta* & *Oenanthe* group, the *Sium* alliance, and the NA endemics clade. The latter two clades formed the closest sister group (Figs. 4 and 5). This was basically consistent with previous studies [11, 12, 14]. The *Sium* alliance clade includes two genera, the *Sium* and the *Cryptotaenia*. Within the *Cryptotaenia*, the populations of *Cryptotaenia japonica* Hassk. gathered a branch, and subsequently formed a sister group to the *Cryptotaenia canadensis* (L.) DC. The *Sium* genus here was highly supported to be split into three branches: *Sium* I, *Sium* II, and *Sium* III. Two high-altitude species [*Sium crispulifolium* (H.Boissieu) Jing Zhou and *S. ventricosum*] clustered together to form the *Sium* I clade. Three species [*S. ninsi*, *Sium tenue* (Kom.) Kom., and *Sium serra* (Franch. & Sav.) Kitag.] gathered *Sium* II. The *Sium* III consist of *Sium suave* Walter and *Sium medium* Fisch. & C.A.Mey. Among these three branches, *Sium* I and *Sium* II were supported to be the closest sister (Figs. 4 and 5a–f), gathering the southern Palearctic clade. This topology structure was consistent with the previous studies that combined nrDNA ITS and cpDNA fragments (*rps16–trnK*) with improved support [12, 14]. Although an alternative result [((*Sium* I, *Sium* III), *Sium* II)] was proved in the phylogenetic analyses inferred from *rps16–trnK* and *trnQ–trnK*, this topology was moderately supported at the key nodes (Fig. 5g–h).

For the *Cicuta* & *Oenanthe* group, the taxa of *Cicuta* and *Oenanthe* each formed a nature branch. The genus *Oenanthe* was strongly supported to be divided into three branches. The relationships among these branches were incontrovertible with *Oenanthe* I and *Oenanthe* II forming the closest sister group with high supports inferred from the whole genome, 78 CDSs, 8 CDSs, and *psbI–trnK* (Figs. 4 and 5). Although the results inferred from the remaining four datasets have only moderate support, the topology is consistent. Two tuberous geophyte species [*Oenanthe pimpinelloides* L. and *Oenanthe virgata* Poir.] were gathered together to form *Oenanthe* III. The *Oenanthe* II consisted of populations of *Oenanthe javanica* (Blume) DC. and divided into two branches. The populations of high-altitude and low-altitude clustered separately (Table S1, Fig. 4). The *Oenanthe* I contained four taxa with narrow leaf blades, two alpine taxa (*Oenanthe hookeri* C.B.Clarke and *Oenanthe thomsonii* C.B.Clarke), *Oenanthe linearis* Wall. ex DC., and *Oenanthe linearis* subsp. *rivularis* (Dunn) C.Y.Wu & F.T.Pu. The interspecific relationships within *Oenanthe* I were ambiguous due to the extremely short differentiated branches of the *Oenanthe* I clade and the depress supports within the clade. Three topologies have been inferred from the eight datasets. Two populations of *O. linearis* subsp. *rivularis* formed a stable branch within *Oenanthe* I. The first topology (i1) reconstructed based on the whole genome, non-coding region, and 9 introns was very stable with the alpine branch well supported to form the closest sister group with *O. linearis* subsp. *rivularis* (Fig. 5a–c). The phylogenetic tree inferred from 78 CDSs has a unique topology (i2) of the *Oenanthe* I:

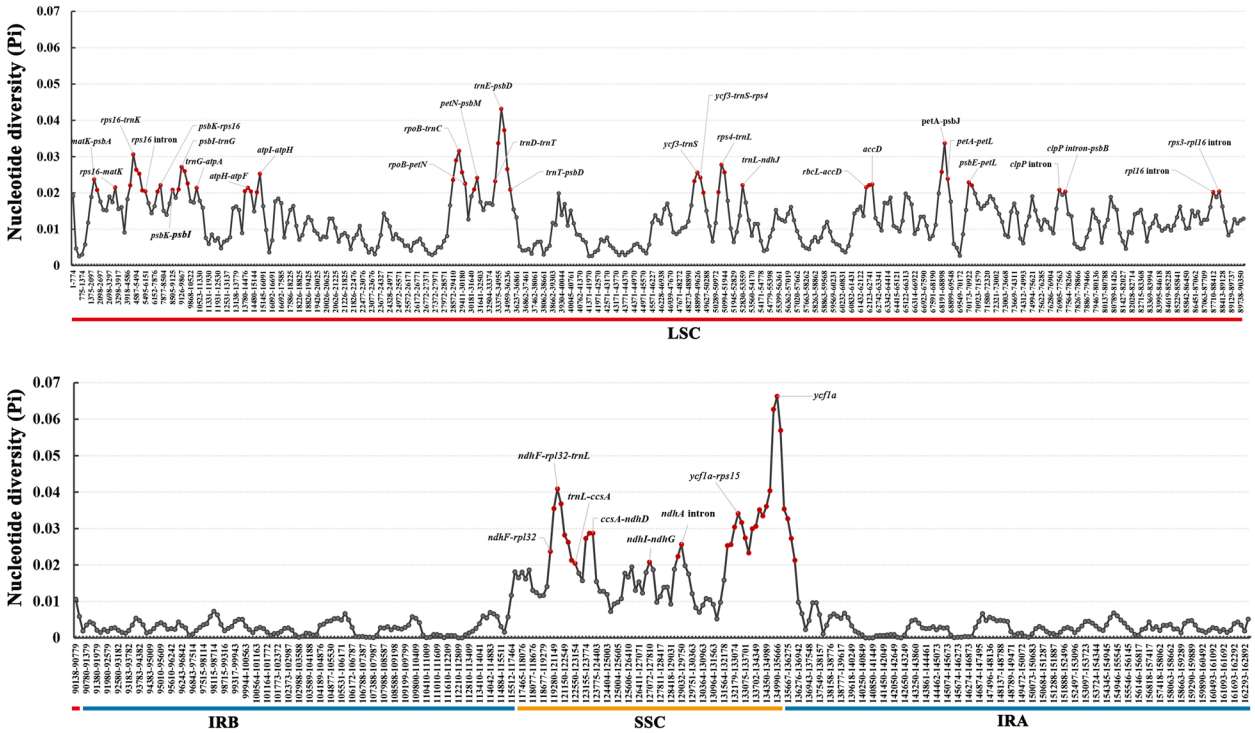

Fig. 2 The nucleotide diversity (Pi) of 30 Oenantheae chloroplast genomes. Regions with high Pi (above 0.02) were marked out

the alpine branch and *O. linearis* were the closest sister groups with very lower supports (BS = 39, PP = 0.85). The remaining datasets shared the third topology (i3), the *O. linearis* and its subspecies clustered together, but the supports were not high (Fig. 5e–h). The interspecific relationships of the genus have been unresolved for a long time, and phylogenetic relationships based on small fragments (nrDNA ITS, cpDNA *rps16–trnK*) have often received poor support in previous studies [1, 11, 12, 14]. Our study provides a basis for resolving the phylogenetic relationships within the genus, to better solve the problem within *Oenanthe* I, we recommend obtaining rich nuclear genes for comprehensive analyses. Populations of the *S. suave*, *C. japonica*, *and C. virosa* were divided with very short branch lengths, with moderate node supports in the four large datasets (whole genome, noncoding region, 9 introns, and 78 CDSs) and very low supports in the four small datasets (Fig. 5).

Our results provided stable phylogenetic relationships among species of Oenantheae except the *Oenanthe* I clade. Molecular data with sufficient non-coding sequences appear to be effective in resolving interspecific relationships within the *Oenanthe* I clade (Fig. 5a–c). However, some additional data may need to be adopted into the study to clarify the relationships between species within the *Oenanthe* I clade. At present, many molecular data have been proposed to resolve generic-level phylogenies, such as single-copy nuclear genes (SCG), low-copies nuclear genes, and SNPs extracted from transcriptome or genome [78–82]. Despite the discordance between nuclear-based and plastid-based phylogenetic trees, sufficiently stable topologies can support a more comprehensive interpretation of taxa evolution [6, 83–85]. The previous phylogenetic analyses of the tribe Oenantheae rarely involved taxa distributed in China [11, 12, 14]. Our research contributes in part to the replenishment of Oenantheae's global resources.

Positively selected gene responses to the adaptive evolution of Oenantheae

We calculated the Ka, Ks, and their ratio Ka/Ks (ω) to evaluate the selection pressure of the 78 PCGs (Table S4). The results showed that the Ka values ranged from 0 to 0.0246 and the Ks values ranged from 0 to 0.0594. Thirteen PCGs (*atpH*, *clpP*, *ndhC*, *petG*, *petL*, *psaI*, *psbD*, *psbE*, *psbF*, *psbI*, *psbL*, *rps7*, and *ycf3*) have Ka = 0, which indicated these PCGs without any non-synonymous mutations. Only one PCG (*psaJ*) with Ks = 0, which suggested this gene has non-synonymous mutations but no synonymous mutations. The Ka/Ks (ω) value of *psaJ* was not calculated because Ks = 0 and the ω value tended to infinity. The ω values for the remaining PCGs ranged from 0 to 1.0161 (Table S4). A total of 12 PCGs were identified with ω values above 0.5

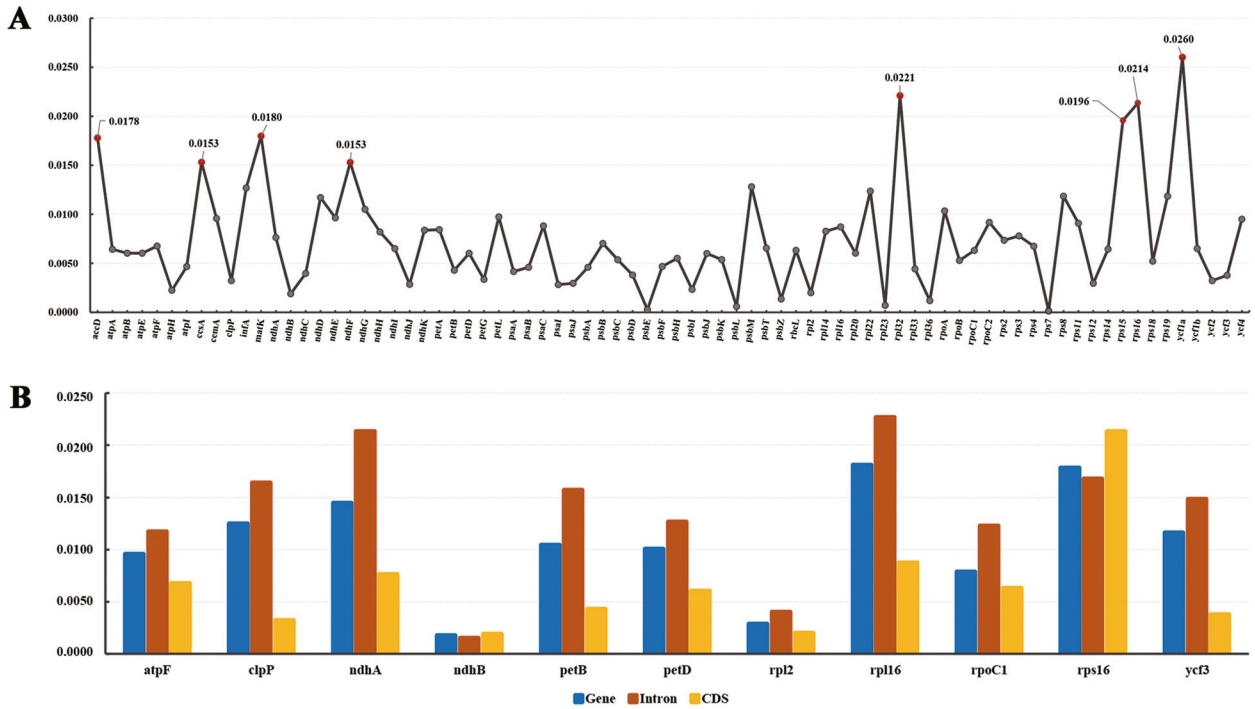

Fig. 3 The nucleotide diversity (Pi) of sequences. **A**, Pi of 78 protein-coding sequences (CDSs), sequences with Pi above 0.015 were marked out. **B**, Pi of 11 protein-coding genes, their CDSs, and introns

(*ccsA*, *matK*, *psbK*, *psaJ*, *rbcL*, *rpl20*, *rpoA*, *rps14*, *rps15*, *ycf1a*, *ycf1b*, and *ycf2*) (Fig. 6). Among these genes, *psaJ* and *ycf2* possessed ω values greater than 1. The results suggested ten PCGs might be under relaxed selection with $0.5 < \omega < 1$ and two genes have undergone strong positive selection.

To detect sites under positive selection in each PCG, we performed tests by comparing null models (M1a and M7) against alternative models (M2a and M8). We have calculated several parameters to estimate the positive selection, including the LRT *P*-values of the compared models (M1a vs. M2a, M7 vs. M8), the detailed log-likelihood values and free parameters of M7 and M8, and the positively selected sites calculated under BEB method (Table S7). The calculation of LRT *P*-values showed that eight PCGs (*accD*, *rbcL*, *rps8*, *ycf1a*, *ycf1b*, *ycf2*, *ndhF*, and *ndhK*) were significant ($P < 0.05$) for both M1a-M2a and M7-M8, two PCGs (*ndhH* and *rps11*) were not significant ($P > 0.05$) for the M1a-M2a comparison but significant under the M7-M8. Based on BEB analysis, sites had probability > 50% for the positive-selection class with $\omega > 1$ were detected in 44 PCGs (Table S7). Among these genes, 14 PCGs (*rpoC2*, *rpl20*, *psbT*, *psaJ*, and the ten PCGs significant under M7-M8 mentioned above) have some positively selected sites with a probability > 95% (Table 2). The LRT of the four PCGs (*rpoC2*, *rpl20*, *psbT*, and *psaJ*) were not significant ($P > 0.05$) for both comparisons although their positively selected sites probability greater than 95%. Sites that had probabilities > 99% were presented in seven PCGs (*rbcL*, *rps8*, *ycf1a*, *ycf1b*, *ycf2*, *ndhF*, and *rps11*).

Our Ka and Ks calculation results have suggested ten PCGs (*ccsA*, *matK*, *psbK*, *rbcL*, *rpl20*, *rpoA*, *rps14*, *rps15*, *ycf1a*, and *ycf1b*) under relaxed selection and two (*psaJ* and *ycf2*) undergone strong positive selection. Among these PCGs, four (*rbcL*, *ycf1a*, *ycf1b*, and *ycf2*) have detected significant positive selection in some sites. The LRTs of these PCGs were significant at a 1% level under both M7-M8 and M1a-M2a tests. Also, the BEB calculation provided strong evidence for sites under positive selection as the posterior probabilities for $\omega > 1$ were high (Table 2). Together, these results suggested strong evidence for sites under positive selection in these four PCGs (*rbcL*, *ycf1a*, *ycf1b*, and *ycf2*). The BEB calculation also provided some evidence for sites under positive selection in PCGs *rpl20* and *psaJ* as the posterior probabilities for $\omega > 1$ were high (probability > 0.95). However, the LRTs of these two PCGs were not significant ($P > 0.05$) for both M7-M8 and M1a-M2a comparisons (Table 2). These situations also existed in the *rpoC2* and *psbT* genes. These results suggested some weak evidence for sites under positive selection in the four PCGs (*rpl20*, *psaJ*, *rpoC2*, and *psbT*). For the remaining six PCGs (*ccsA*, *matK*, *psbK*, *rpoA*, *rps14*, and *rps15*), the LRT *P*-values

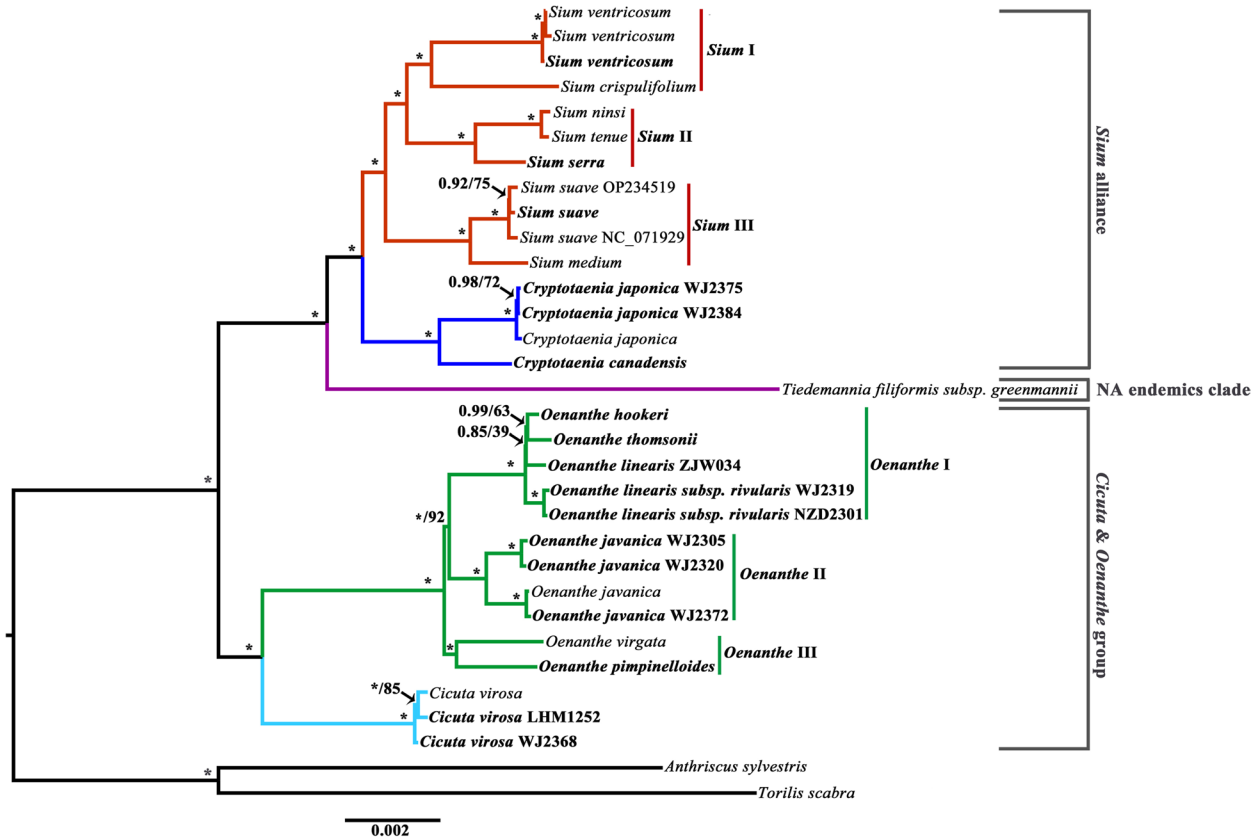

Fig. 4 Phylogenetic relationships inferred from 32 species based on 78 shared CDSs. Support values marked above the branches follow the order Bayesian inference (PP, posterior probability)/maximum likelihood (BS, bootstrap support), * represent the best support (100%). Species names in bold indicate that these species are newly sequenced

were above 0.05 for both two comparisons, and the BEB calculation only provided weak evidence for sites under positive selection as the posterior probability for $\omega > 1$ was low (< 95%) and the posterior distribution for ω was diffuse at every site (Table S7). All these suggested that these six PCGs might be under weak positive selection. *Site* models have detected extra four PCGs (*accD*, *rps8*, *ndhF*, and *ndhK*) possessing significant positively selected sites. Both the LRT and BEB calculations have provided strong evidence. The tests for sites under positive selection in the *ndhH* and *rps11* genes were equivocal with the M1a-M2a and M7-M8 comparison giving conflicting results. We tend to accept the test of M1a-M2a because this test is noted to be more stringent when the evidence for positive selection exists but is not very strong [56, 86]. These results together suggested some evidence for sites under positive selection in the *ndhH* and *rps11* genes, although this evidence was not very strong.

Tribe Oenantheae has a high proportion of bog and water species relative to terrestrial members. The occupation of the aquatic environments indicates that Oenantheae species have adapted to conditions of damp, marshy, or truly aquatic habitats. Compared with terrestrial species, emergent aquatic plants occupy stressful ecological habitats characterized by low light, and reduced carbon and oxygen availability [87]. Survival in aquatic habitats has resulted in adaptations specific to low oxygen concentrations. Plants of the tribe Oenantheae exhibit various adaptations to these habitats, such as clusters of fibrous or tuberous roots and corky-thickened fruits [7, 11]. Here possible evidence of positive selection in chloroplast coding genes was detected to reveal the adaptation of Oenantheae species to aquatic environments at the molecular level. Based on our results, a total of eight genes (*accD*, *rbcL*, *rps8*, *ycf1a*, *ycf1b*, *ycf2*, *ndhF*, and *ndhK*) are considered positive selection genes. Gene *accD* encodes the beta carboxyl transferase subunit of ACCase and has been verified to affect several biological processes such as storage compound metabolism, leaf and seed development [88–91]. The two significantly positively selected sites we detected in the *accD* gene varied mainly between the *Cicuta* & *Oenanthe* group and the other species. We identified these genes as possibly associated with the unique traits *Cicuta* & *Oenanthe*

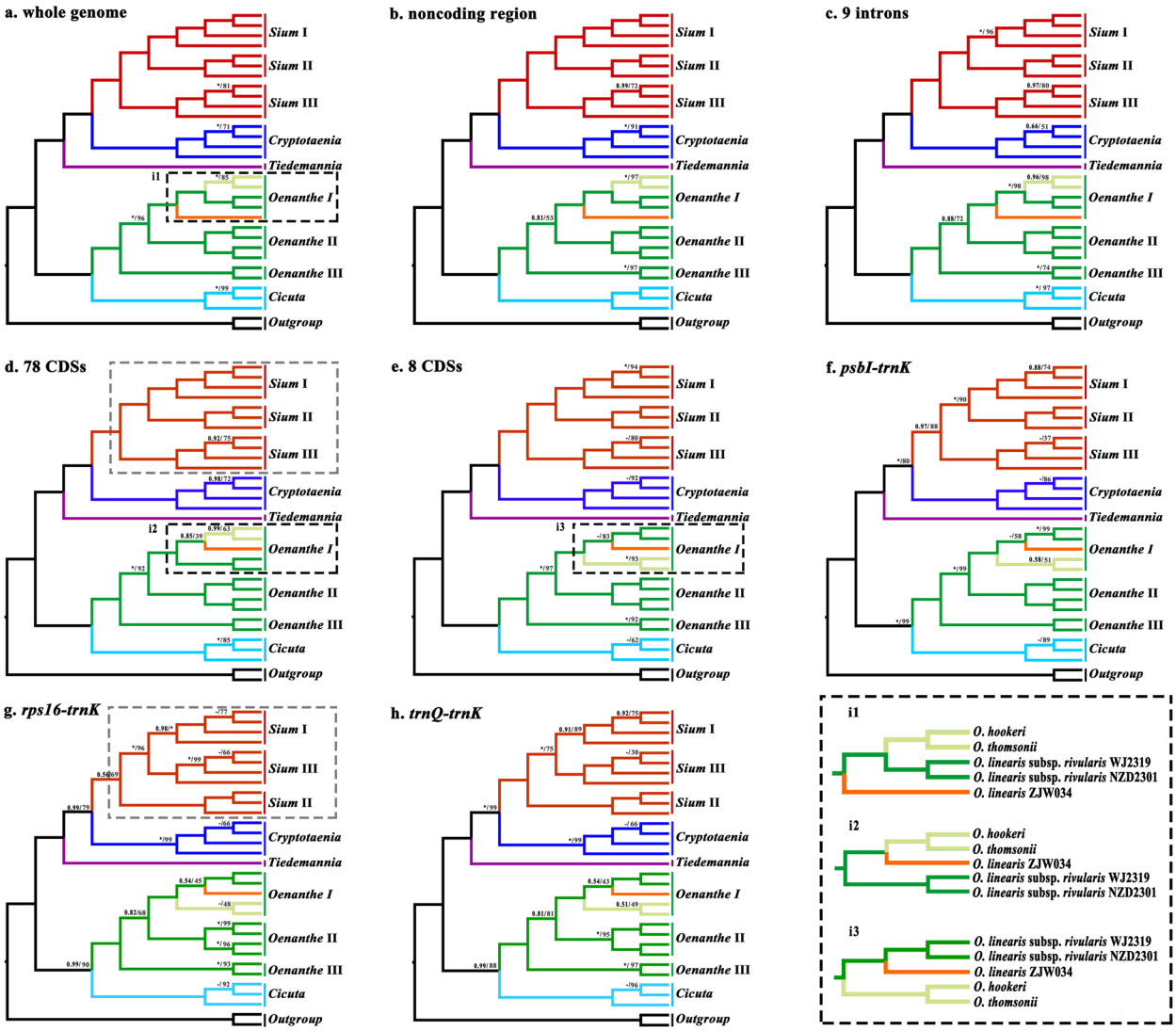

Fig. 5 Comparison of eight phylogenetic trees. Phylogenetic tree each inferred from **a**, the whole genome matrix; **b**, the noncoding region concatenated matrix; **c**, 9 introns concatenated matrix; **d**, 78 CDSs concatenated matrix; **e**, eight CDSs concatenated matrix; **f**, *psbI–trnK*; **g**, *rps16–trnK*; **h**, *trnQ–trnK*. Support values marked above the branches follow the order Bayesian inference (PP, posterior probability)/maximum likelihood (BS, bootstrap support), * represent the best support (100%), - represent PP values < 50%. In the black dotted box at the bottom right are the three topologies of the *Oenanthe I* clade

group owned particularly in leaf and seed development. We have found statistically that the leaf and fruit morphology of *Oenanthe* and *Cicuta* are different from other groups. The leaf blades of these two genera species always have one or more pinnates. The fruits of them are overall ovoid with thick and corky fruit ribs, with vittae solitary in each furrow and 2 on commissure [7, 18, 92–95]. The chloroplast ribosomal proteins act as important constituents of protein synthesis machinery and participate in various processes of plant growth, and development as well as reaction to unfavorable conditions [96–99]. Adaptive evolution of the *rps8* gene may be helpful for the normal growth and development of Oenantheae species in aquatic environments. The remaining six positive selection genes are functionally associated with photosynthesis. The *rbcL* gene encodes the Rubisco large subunit, which catalyzes the assimilation of atmospheric CO2 during photosynthesis [100–102]. Positive selection of this gene has been detected in some plants and suggested adaptation to low CO2 concentration, shade-tolerant, and aquatic environments [32, 60, 103, 104], but not prevalent in the Apiaceae. We detected ten positive selection sites in the *rbcL* gene, the increased amino acid replacement may reflect the continuous fine-tuning of

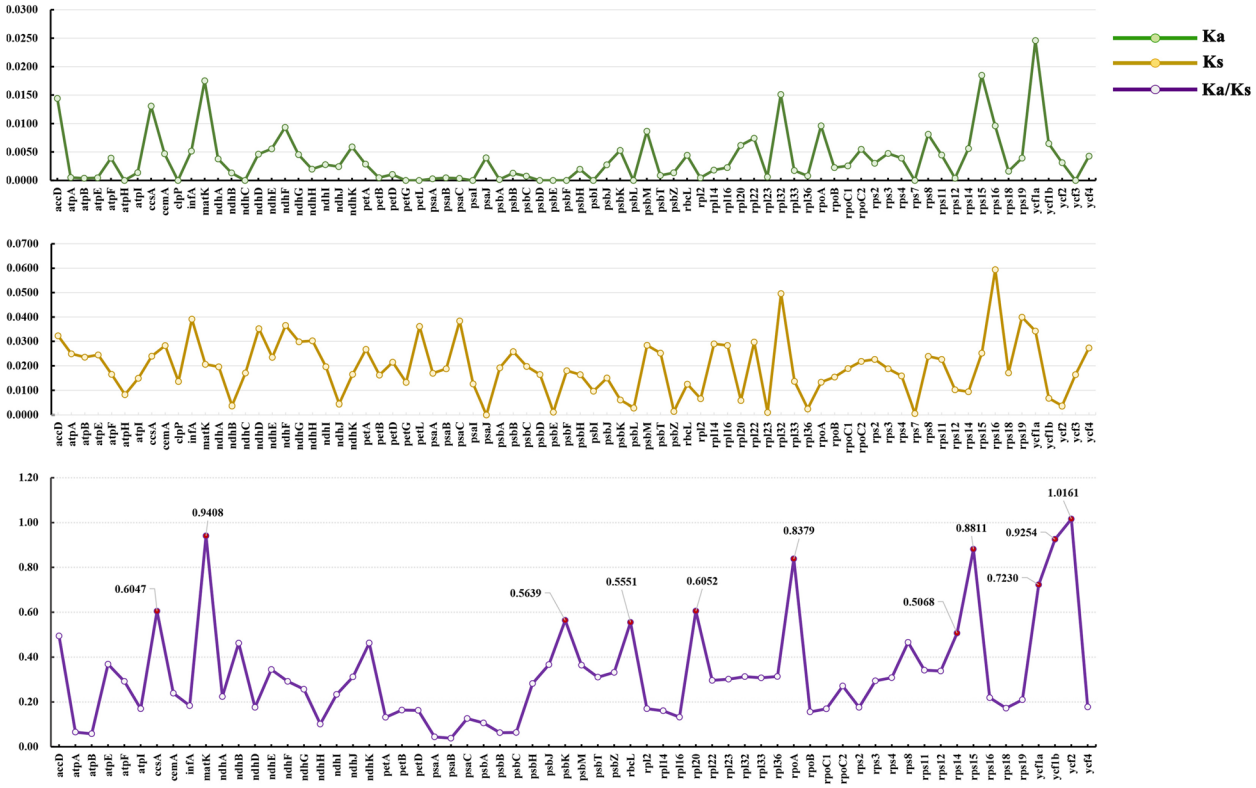

Fig. 6 The average Ka, Ks, and Ka/Ks values curves of the protein-coding sequences (CDS). CDSs with Ka/Ks > 0.5 were marked out with red circles in the Ka/Ks curve

Rubisco under varying species' ecological conditions. The *ndh* genes (*ndhF* and *ndhK*) encode NADH-dehydrogenase subunits of the Ndh1-complex bound to the thylakoid membrane, which were fundamental to the electron transport chain for the generation of ATP, and photosynthesis of plants [105–108]. Positive selection of these two *ndh* genes may reflect the adaptation to aquatic environments stress, such as low light and reduced oxygen availability. Positive selections of these two genes in Apiaceae have been detected commonly [24, 36, 109]. Essential genes *ycf1* and *ycf2* in plant chloroplast genomes encode proteins that are indispensable for cell survival and photosynthesis [110–112]. Overall, positive selection of the eight chloroplasts protein-coding genes (*accD*, *rbcL*, *rps8*, *ycf1a*, *ycf1b*, *ycf2*, *ndhF*, and *ndhK*) may be responses to aquatic environment adaptation of Oenantheae species. There may be partial positive selection in six genes that with positive selection sites (posterior probability above 95%), including *rpl20*, *psaJ*, *rpoC2*, *psbT*, *ndhH*, and *rps11*, but it is not statistically significant. Nevertheless, we suggest that these genes still require attention because they may be potential positive selection genes.

Conclusion

In conclusion, we generated the complete chloroplast genomes of 17 Oenantheae species. A deep comparative analysis of 30 Oenantheae chloroplast genomes has been conducted to create an accurate map of the genomic structure of hydrophytic umbellifers. A total of 30 regions (*matK–psbA*, *rps16–matK*, *rps16* intron–*trnK*, *rps16* intron, *rps16* intron–*psbK*, *psbK–psbI*, *psbI–trnS–trnG*, *trnG–atpA*, *atpH–atpF* intron, *atpI–atpH*, *rpoB–trnC–petN*, *petN–psbM*, *trnD–trnY–trnE–trnT–psbD*, *ycf3–trnS–rps4*, *rps4–trnT–trnL*, *trnL–trnF–ndhJ*, *rbcL–accD*, *accD*, *petA–psbJ–psbL*, *psbE–petL*, *clpP* intron, *clpP* intron–*psbB*, *rpl16* intron, *rps3–rpl16* intron, *ndhF–rpl32–trnL–ccsA*, *ccsA–ndhD*, *ndhI–ndhG*, *ndhA* intron, *ycf1a–rps15–ndhH*, and *ycf1a* gene) have been identified with high nucleotide diversity (Pi > 0.02), which suggested to be mutation hotspot regions among Oenantheae species. Among these, the *ycf1a* gene, *trnE–trnT–psbD*, *ndhF–rpl32–trnL*, *rpoB–trnC*, *ycf1a–rps15*, *petA–psbJ*, and *rps16* intron–*trnK* regions were considered as candidate barcodes for the phylogenetic analyses of Oenantheae due to well aligned and rich informative sites. Eight genes

Table 2 Positive selected sites identified in the chloroplast genomes of Oenantheae

Gene name	LRT *P*-value		Positively selected sites (BEB, *: PP > 95%; **: PP > 99%)	sites number
	M7 (beta) vs. M8 (beta&ω)	M1a (nearly neutral) vs. M2a (positive selection)		
accD	0.000004515	0.000000015	100 H 0.983*,207 K 0.954*	2
rbcL	0.000000000	0.000000000	28 D 0.974*,91 A 1.000**,95 N 0.997**,97 Y 0.998**,225 I 0.997**,309 I 0.998**,328 S 1.000**,354 I 0.956*,355 A 0.972*,443 E 0.998**	10
rps8	0.000000000	0.000000000	57 D 1.000**	1
ycf1a	0.000000000	0.000000000	469 R 0.960*, 795 V 0.982*,1014 K 0.971*,1085 I 0.969*,1092 K 1.000**,1093 I 0.965*,1094 L 0.986*,1111 Y 0.962*	8
ycf2	0.000000000	0.000000000	103 F 1.000**,503 Q 0.996**,746 L 0.996**,833 R 0.955*,915 P 0.950*,1025 Q 0.951*	6
ycf1b	0.000000888	0.000000131	200 S 0.976*,205 K 0.994**,206 Y 0.980*,215 R 0.975*,217 S 0.975*,244 N 0.971*,270 K 1.000**	7
ndhF	0.000004851	0.000065086	465 Q 0.988*,655 N 0.952*,663 C 1.000**	3
ndhH	0.003524280	0.082768146	198 I 0.960*	1
ndhK	0.011201551	0.022716790	181 F 0.964*,218 K 0.957*	2
rps11	0.012214628	0.054106065	14 G 0.993**	1
rpoC2	0.082830660	0.347241769	239 I 0.969*	1
rpl20	0.096456032	0.117651549	12 R 0.964*	1
psbT	0.225892513	0.225960517	33 K 0.972*	1
psaJ	0.422979316	0.423014425	10 V 0.977*,14 L 0.977*,36 A 0.977*	3

(*accD*, *rbcL*, *rps8*, *ycf1a*, *ycf1b*, *ycf2*, *ndhF*, and *ndhK*) with strong signatures of positive selection were convincingly detected. Two (*accD* and *rps8*) are related to plant growth and development, and the remaining are mainly related to the photosynthesis system. Such a comparative genomic analysis of the Oenantheae chloroplast genomes offers us an unprecedented opportunity to reveal footprints of the adaptive evolution of chloroplast genes that make Oenantheae species adapt to aquatic environments. Our phylogenetic analyses also recovered reliable relationships among species of Oenantheae except within the *Oenanthe* I clade. Phylogeny and evolution of the genus *Oenanthe* may be further clarified by incorporating more nuclear genes in further studies. In addition, expanding species sampling of North American endemic species will contribute to a deeper understanding of the molecular adaptive evolution of Oenantheae. Our research only serves as an introduction, and we urge other researchers to join us in the future.

Supplementary Information

The online version contains supplementary material available at https://doi.org/10.1186/s12870-024-05863-2.

Supplementary Material 1.
Supplementary Material 2.
Supplementary Material 3.
Supplementary Material 4.
Supplementary Material 5.
Supplementary Material 6.
Supplementary Material 7.
Supplementary Material 8.
Supplementary Material 9.
Supplementary Material 10.
Supplementary Material 11.
Supplementary Material 12.
Supplementary Material 13.
Supplementary Material 14.
Supplementary Material 15.
Supplementary Material 16.
Supplementary Material 17.
Supplementary Material 18.
Supplementary Material 19.
Supplementary Material 20.

Acknowledgements
We are grateful to the China National Botanical Garden in Beijing and the Yaoluoping Nature Reserve in Anhui Province for allowing us to collect plant material. We would like to thank Zhu Xin-Xin from Xinyang Normal University for providing information on the distribution of some materials.

Author contributions
Conceptualization, WJ and SCF; validation, WBC, LHM, ZW, YJX; interpretation of data, ZJW and MXD; analysis, WJ and YJX; writing—original draft preparation, WJ; writing—review and editing, SCF and WJ; funding acquisition, WJ. All authors have read and agreed to the published version of the manuscript.

Funding
This work was supported by the National Natural Science Foundation of China (Grant no. 32200191), the Foundation of Jiangsu Key Laboratory for the Research and Utilization of Plant Resources (JSPKLB202214).

Data availability
The datasets generated and analyzed during the current study are available in the NCBI (https://www.ncbi.nlm.nih.gov) repository. The raw reads have been submitted to GenBank at NCBI BioProject PRJNA1154308, with SRA numbers SRR30524793–SRR30524809. The assembly and annotated chloroplast genomes were deposited in NCBI with accession numbers PQ283862–PQ283878. Voucher specimens were identified by Jun Wen and deposited in NAS (Herbarium, Institute of Botany, Chinese Academy of Sciences, Jiangsu Province) with deposition numbers (NAS00640404– NAS00640420, Fig. S3).

Declarations

Ethics approval and consent to participate
Not applicable.

Consent for publication
Not applicable.

Competing interests
The authors declare no competing interests.

Received: 10 September 2024 Accepted: 22 November 2024
Published online: 28 November 2024

References

1. Banasiak Ł, Piwczyński M, Uliński T, Downie SR, Watson MF, Shakya B, et al. Dispersal patterns in space and time: a case study of Apiaceae subfamily Apioideae. J Biogeogr. 2013;40:1324–35.
2. Zhou J, Gong X, Downie SR, Peng H. Towards a more robust molecular phylogeny of Chinese Apiaceae subfamily Apioideae: additional evidence from nrDNA ITS and cpDNA intron (*rpl*16 and *rps*16) sequences. Mol Phylogenet Evol. 2009;53:56–68.
3. Clarkson JJ, Zuntini AR, Maurin O, Downie SR, Plunkett GM, Nicolas AN, et al. A higher-level nuclear phylogenomic study of the carrot family (Apiaceae). Am J Bot. 2021;108:1–18.
4. Downie SR, Katz-Downie DS, Watson MF. A phylogeny of the flowering plant family Apiaceae based on chloroplast DNA *rpl*16 and *rpo*C1 intron sequences: towards a suprageneric classification of subfamily Apioideae. Am J Bot. 2000;87:273–92.
5. Downie SR, Spalik K, Katz-Downie DS, Reduron JP. Major clades within Apiaceae subfamily Apioideae as inferred by phylogenetic analysis of nrDNA ITS sequences. Plant Div Evol. 2010;128:111–36.
6. Wen J, Xie DF, Price M, Ren T, Deng YQ, Gui LJ, et al. Backbone phylogeny and evolution of Apioideae (Apiaceae): new insights from phylogenomic analyses of plastome data. Mol Phylogenet Evol. 2021;161:107183.
7. Wen J, Yu Y, Xie DF, Peng C, Liu Q, Zhou SD, et al. A transcriptome-based study on the phylogeny and evolution for taxonomic controversial subfamily Apioideae (Apiaceae). Ann Bot-London. 2020;125:937–53.
8. Shu P, Sheh ML. Pollen photographs and flora of umbelliferae in China. Shanghai: Shanghai Scientific and Technical Publishers; 2001.
9. Xi YZ, Sun XJ. Pollen morphology of Umbelliferae in China and its evolution. In: The Institute of Botany Academia Sinica, editor. Botanical Research, No. 1. Beijing: Science Press; 1983. p. 57–83.
10. Hardway TM, Spalik K, Watson MF, Katz-Downie DS, Downie SR. Circumscription of Apiaceae tribe Oenantheae. S Afr J Bot. 2004;70:393–406.
11. Downie SR, Katz-Downie DS, Sun FJ, Lee CS. Phylogeny and biogeography of Apiaceae tribe Oenantheae inferred from nuclear rDNA ITS and cpDNA psbI–5'trnK(uuu) sequences, with emphasis on the north American endemics clade. Botany. 2008;86:1039–64.
12. Spalik K, Banasiak Ł, Feist MAE, Downie SR. Recurrent short-distance dispersal explains wide distributions of hydrophytic umbellifers (Apiaceae tribe Oenantheae). J Biogeogr. 2014;41:1559–71.
13. Desjardins SD, Leslie AC, Stace CA, Schwarzacher T, Bailey JB. Intergeneric hybridisation between *Berula erecta* and *helosciadium nodiflorum* (Apiaceae). Taxon. 2015;64:784–94.
14. Spalik K, Downie SR, Watson MF. Generic delimitations within the *Sium* alliance (Apiaceae tribe Oenantheae) inferred from cpDNA *rps*16-5'*trn*K(UUU) and nrDNA ITS sequences. Taxon. 2009;58:735–48.
15. Plants of the World Online. Facilitated by the Royal Botanic Gardens, Kew. Published on the Internet. http://www.plantsoftheworldonline.org/. Retrieved 10 Sept 2024.
16. Spalik K, Downie SR. The evolutionary history of *Sium Sensu Lato* (Apiaceae): dispersal, vicariance, and domestication as inferred from ITS rDNA phylogeny. Am J Bot. 2006;93:747–61.
17. Spalik K, Downie SR. Intercontinental disjunctions in *Cryptotaenia* (Apiaceae, Oenantheae): an appraisal using molecular data. J Biogeogr. 2007;34:2039–54.
18. Feist MAE, Downie SR, Magee AR, Liu MR. Revised generic delimitations for *Oxypolis* and *Ptilimnium* (Apiaceae) based on leaf morphology, comparative fruit anatomy, and phylogenetic analysis of nuclear rDNA ITS and cpDNA *trn*Q-*trn*K intergenic spacer sequence data. Taxon. 2012;61:402–18.
19. Feist MAE, Downie SR. A phylogenetic study of *Oxypolis* and *Ptilimnium* based on nuclear rDNA ITS sequences. Syst Bot. 2008;33:447–58.
20. Bone TS, Downie SR, Affolter JM, Spalik K. A phylogenetic and biogeographic study of the genus *Lilaeopsis* (Apiaceae tribe Oenantheae). Syst Bot. 2011;36:789–805.
21. Lee CS, Downie SR. Phylogenetic relationships within *Cicuta* (Apiaceae tribe Oenantheae) inferred from nuclear rDNA ITS and cpDNA sequence data. Can J Bot. 2006;84:453–68.
22. Downie SR, Sun FJ, Katz-Downie DS, Colletti GJ. A phylogenetic study of *Perideridia* (Apiaceae) based on nuclear ribosomal DNA ITS sequences. Syst Bot. 2004;29:737–51.
23. Zhou BF, Yuan S, Crowl AA, Liang YY, Shi Y, Chen XY, et al. Phylogenomic analyses highlight innovation and introgression in the continental radiations of Fagaceae across the Northern Hemisphere. Nat Commun. 2022;13:1320.
24. Peng C, Guo XL, Zhou SD, He XJ. Backbone phylogeny and adaptive evolution of *Pleurospermum* s. l.: new insights from phylogenomic analyses of complete plastome data. Front Plant Sci. 2023;14:1148303.
25. Ma XG, Ren YB, Sun H. Introgression and incomplete lineage sorting blurred phylogenetic relationships across the genomes of sclerophyllous oaks from southwest China. Cladistics. 2024;40:357–73.
26. Li QQ, Khasbagan, Zhang ZP, Wen J, Yu Y. Plastid phylogenomics of the tribe potentilleae (Rosaceae). Mol Phylogenet Evol. 2024;190:107961.
27. Wang J, Kan S, Liao X, Zhou J, Tembrock LR, Daniell H, et al. Plant organellar genomes: much done, much more to do. Trends Plant Sci. 2024;29:754–69.
28. Zeng ZH, Zhong L, Sun HY, Wu ZK, Wang X, Wang H, et al. Parallel evolution of morphological and genomic selfing syndromes accompany the breakdown of heterostyly. New Phytol. 2024;242:302–16.
29. Liu LJ, Liu CK, Cai J, Deng JJ, He XJ, Zhou SD. The complete plastomes of thirteen *Libanotis* (Apiaceae, Apioideae) plants: comparative and phylogenetic analyses provide insights into the plastome evolution and taxonomy of *Libanotis*. BMC Plant Biol. 2024;24:106.
30. Song BN, Liu CK, Zhao AQ, Tian RM, Xie DF, Xiao YL, et al. Phylogeny and diversification of genus *Sanicula* L. (Apiaceae): novel insights from plastid phylogenomic analyses. BMC Plant Biol. 2024;24:70.
31. Zhang X, Sun Y, Landis JB, Lv Z, Shen J, Zhang H, et al. Plastome phylogenomic study of Gentianeae (Gentianaceae): widespread gene tree discordance and its association with evolutionary rate heterogeneity of plastid genes. BMC Plant Biol. 2020;20:340.
32. Li QQ, Zhang ZP, Aogan, Wen J. Comparative chloroplast genomes of *Argentina* species: genome evolution and phylogenomic implications. Front Plant Sci. 2024;15:1349358.
33. Wen J, Wu BC, Li HM, Zhou W, Song CF. Plastome structure and phylogenetic relationships of genus *Hydrocotyle* (Apiales): provide insights into the plastome evolution of *Hydrocotyle*. BMC Plant Biol. 2024;24:778.
34. Liu CK, Deng JJ, Song BN, Qin HH, Zhou SD, He XJ. Plastid phylogenomics provide evidence to accept a new genus *Pseudopeucedanum* (Apiaceae) separated from *Peucedanum s.l.* Bot J Linn Soc. 2023;205:243–52.
35. Tian R, Aou X, Song B, Li Z, He X, Zhou S. Plastid phylogenomic analyses reveal a cryptic species of *Ligusticopsis* (Apiaceae, Angiosperms). Int J Mol Sci. 2023;24:7419.
36. Qin HH, Cai J, Liu CK, Zhou RX, Price M, Zhou SD, et al. The plastid genome of twenty-two species from *Ferula*, *Talassia*, and *Soranthus*:

comparative analysis, phylogenetic implications, and adaptive evolution. BMC Plant Biol. 2023;23:9.
37. Gui LJ, Xie DF, Peng C, Ren T, Yu LY, Zhou SD, He XJ. Chloroplast genomes and ribosomal DNA provide insights into divergence and morphological evolution of alpine *Tongoloa*. J Syst Evol. 2023. https://doi.org/10.1111/jse.13028.
38. Downie SR, Jansen RK. A comparative analysis of whole plastid genomes from the Apiales: expansion and contraction of the inverted repeat, mitochondrial to plastid transfer of DNA, and identification of highly divergent noncoding regions. Syst Bot. 2015;40:336–51.
39. Spooner DM, Ruess H, Iorizzo M, Senalik D, Simon P. Entire plastid phylogeny of the carrot genus (*Daucus*, Apiaceae): concordance with nuclear data and mitochondrial and nuclear DNA insertions to the plastid. Am J Bot. 2017;104:296–312.
40. Luo L, Yu Y. The complete chloroplast genome of *Cryptotaenia japonica*. Mitochondrial DNA B. 2019;4:1650–1.
41. Zhang Z, Dong H, Yuan M, Yu Y. The complete chloroplast genome of *Oenanthe javanica*. Mitochondrial DNA B. 2020;5:3151–3.
42. Zhou J, Niu JM, Wang XY, Yue JR, Zhou SL, Liu ZW. Plastome evolution in the genus *Sium* (Apiaceae, Oenantheae) inferred from phylogenomic and comparative analyses. BMC Plant Biol. 2023;23:368.
43. Andrews S, Lindenbaum P, Howard B, Ewels P. FastQC: a quality control tool for high throughput sequence data. Cambridge (UK): The Babraham Institute; 2011.
44. Dierckxsens N, Mardulyn P, Smits G. NOVOPlasty: denovo assembly of organelle genomes from whole genome data. Nucleic Acids Res. 2017;45:e18.
45. Lohse M, Drechsel O, Kahlau S, Bock R. Organellargenomedraw–a suite of tools for generating physical maps of plastid and mitochondrial genomes and visualizing expression data sets. Nucleic Acids Res. 2013;41:575–81.
46. Darling ACE, Mau B, Blattner FR, Perna NT, Mauve. Multiple alignment of conserved genomic sequence with rearrangements. Genome Res. 2004;14:1394–403.
47. Katoh K, Standley DM. MAFFT multiple sequence alignment software version 7: improvements in performance and usability. Mol Biol Evol. 2013;30:772–80.
48. Rozas J, Ferrer-Mata A, Sanchez-DelBarrio JC, Guirao-Rico S, Librado P, Ramos-Onsins SE, et al. DnaSP 6: DNA sequence polymorphism analysis of large data sets. Mol Biol Evol. 2017;34:3299–302.
49. Yang Z, Nielsen R. Codon-substitution models for detecting molecular adaptation at individual sites along specific lineages. Mol Biol Evol. 2002;19:908–17.
50. Kumar S, Stecher G, Tamura K. MEGA7: Molecular Evolutionary Genetics Analysis version 7.0 for bigger datasets. Mol Biol Evol. 2016;33:1870–4.
51. Stamatakis A. RAxML version 8: a tool for phylogenetic analysis and post-analysis of large phylogenies. Bioinformatics. 2014;30:1312–3.
52. Gao FL, Chen CJ, Arab DA, Du ZG, He YH, Ho SYW. EasyCodeML: a visual tool for analysis of selection using CodeML. Ecol Evol. 2019;9:3891–8.
53. Nielsen R, Yang Z. Likelihood models for detecting positively selected amino acid sites and applications to the HIV-1 envelope gene. Genetics. 1998;148:929–36.
54. Yang Z, Nielsen R, Goldman N, Pedersen AMK. Codon-substitution models for heterogeneous selection pressure at amino acid sites. Genetics. 2000;155:431–49.
55. Yang Z. PAML 4: phylogenetic analysis by maximum likelihood. Mol Biol Evol. 2007;24:1586–91.
56. Álvarez-Carretero S, Kapli P, Yang Z. Beginner's guide on the Use of PAML to detect positive selection. Mol Biol Evol. 2023;40:msad041.
57. Yang Z, Wong WS, Nielson R. Bayes empirical Bayes inference of amino acid sites under positive selection. Mol Biol Evol. 2005;22:1107–18.
58. Hou ZC, Xu GY, Su Z, Yang N. Purifying selection and positive selection on the myxovirus resistance gene in mammals and chickens. Gene. 2007;396:188–95.
59. Figueiró HV, Li G, Trindade FJ, Assis J, Pais F, Fernandes G, et al. Genome-wide signatures of complex introgression and adaptive evolution in the big cats. Sci Adv. 2017;3:e1700299.
60. Gao LZ, Liu YL, Zhang D, Li W, Gao J, Liu Y, et al. Evolution of *Oryza* chloroplast genomes promoted adaptation to diverse ecological habitats. Commun Biol. 2019;2:278.
61. Ren T, Li ZX, Xie DF, Gui LJ, Peng C, Wen J, et al. Plastomes of eight *Ligusticum* species: characterization, genome evolution, and phylogenetic relationships. BMC Plant Biol. 2020;20:519.
62. Zhao L, Zhou W, He J, Li DZ, Li HT. Positive selection and relaxed purifying selection contribute to rapid evolution of male-biased genes in a dioecious flowering plant. Elife. 2024;12:RP89941.
63. Ronquist F, Teslenko M, van der Mark P, Ayres D, Darling A, Ohna SH, et al. MrBayes 3.2: efficient bayesian phylogenetic inference and model choice across a large model space. Sys Biol. 2012;61:539–42.
64. Darriba D, Taboada GL, Doallo R, Posada D. jModelTest 2: more models, new heuristics and parallel computing. Nat Methods. 2012;9:772.
65. Rambaut A. FigTree v1.4. University of Edinburgh, Edinburgh, UK. 2012. http://tree.bio.ed.ac.uk/software/gtree/.
66. Kang L, Xie D, Xiao Q, Peng C, Yu Y, He X. Sequencing and analyses on chloroplast genomes of *tetrataenium candicans* and two allies give new insights on structural variants, DNA barcoding and phylogeny in Apiaceae subfamily Apioideae. PeerJ. 2019;7:e8063.
67. Wang M, Wang X, Sun J, Wang Y, Ge Y, Dong W, et al. Phylogenomic and evolutionary dynamics of inverted repeats across *Angelica* Plastomes. BMC Plant Biol. 2021;21:26.
68. Li ZX, Guo XL, Price M, Zhou SD, He XJ. Phylogenetic position of *Ligusticopsis* (Apiaceae, Apioideae): evidence from molecular data and carpological characters. Aob Plants. 2022;14:plac008.
69. Samigullin T, Logacheva M, Terentieva E, Degtjareva G, Pimenov M, Valiejo-Roman C. Plastid phylogenomic analysis of tordylieae tribe (Apiaceae, Apioideae). Plants. 2022;11:709.
70. Weng L, Jiang Y, Wang Y, Zhang X, Zhou P, Wu M, et al. Chloroplast genome characteristics and phylogeny of the *sinodielsia* clade (apiaceae: apioideae). BMC Plant Biol. 2023;23:284.
71. Downie SR, Watson MF, Spalik K, Katz-Downie DS. Molecular systematics of Old World Apioideae (Apiaceae): relationships among some members of tribe *Peucedaneae* Sensu Lato, the placement of several island-endemic species, and resolution within the apioid superclade. Can J Bot. 2000;78:506–28.
72. Calviño CI, Teruel FE, Downie SR. The role of the Southern Hemisphere in the evolutionary history of Apiaceae, a mostly north temperate plant family. J Biogeogr. 2016;43:398–409.
73. Calviño CI, Tilney PM, van Wyk BE, Downie SR. A molecular phylogenetic study of southern African Apiaceae. Am J Bot. 2006;93:1828–47.
74. Liao C, Downie SR, Li Q, Yu Y, He X, Zhou B. New insights into the phylogeny of *Angelica* and its allies (Apiaceae) with emphasis on east Asian species, inferred from nrDNA, cpDNA, and morphological evidence. Syst Bot. 2013;38:266–81.
75. Fernández M, Ezcurra C, Calviño CI. Chloroplast and ITS phylogenies to understand the evolutionary history of southern South American Azorella, Laretia and *Mulinum* (Azorelloideae, Apiaceae). Mol Phylogenet Evol. 2017;108:1–21.
76. Liu CK, Lei JQ, Jiang QP, Zhou SD, He XJ. The complete plastomes of seven *Peucedanum* plants: comparative and phylogenetic analyses for the *Peucedanum* Genus. BMC Plant Biol. 2022;22:101.
77. Panahi M, Banasiak Ł, Piwczyński M, Puchałka R, Oskolski AA, Spalik K. Phylogenetic relationships among *Dorema*, *Ferula* and *Leutea* (Apiaceae: Scandiceae: Ferulinae) inferred from nrDNA ITS and cpDNA noncoding sequences. Taxon. 2015;64:770–83.
78. Jin ZT, Ma DK, Liu GN, Hodel RGJ, Jiang Y, Ge BJ, et al. Advancing *Pyrus* phylogeny: deep genome skimming-based inference coupled with paralogy analysis yields a robust phylogenetic backbone and an updated infrageneric classification of the pear genus (Maleae, Rosaceae). Taxon. 2024;73:784–99.
79. Messeder JVS, Carlo TA, Zhang G, Tovar JD, Arana C, Huang J, et al. A highly resolved nuclear phylogeny uncovers strong phylogenetic conservatism and correlated evolution of fruit color and size in *Solanum* L. New Phytol. 2024;243:765–80.
80. Hu XZ, Guo C, Qin SY, Li DZ, Guo Z-H. Deep genome skimming reveals the hybrid origin of *Pseudosasa Gracilis* (Poaceae: Bambusoideae). Plant Diversty. 2024;46:344–52.
81. Liu JX, Guo C, Ma PF, Zhou MY, Luo YH, Zhu GF, et al. The origin and morphological character evolution of the paleotropical woody bamboos. J Integr Plant Biol. 2024. https://doi.org/10.1111/jipb.13751.
82. Wei ZR, Jiao D, Wehenkel CA, Wei XX, Wang XQ. Phylotranscriptomic and ecological analyses reveal the evolution and morphological

adaptation of *Abies*. J Integr Plant Biol. 2024. https://doi.org/10.1111/jipb.13760.
83. Liu BB, Ren C, Kwak M, Hodel RGJ, Xu C, He J, et al. Phylogenomic conflict analyses in the apple genus *Malus* s.l. reveal widespread hybridization and allopolyploidy driving diversification, with insights into the complex biogeographic history in the Northern Hemisphere. J Integr Plant Biol. 2022;64:1020–43.
84. Jin ZT, Hodel RGJ, Ma DK, Wang H, Liu GN, Ren C, et al. Nightmare or delight: taxonomic circumscription meets reticulate evolution in the phylogenomic era. Mol Phylogenet Evol. 2023;189: 107914.
85. Zhang G, Ma H. Nuclear phylogenomics of angiosperms and insights into their relationships and evolution. J Integr Plant Biol. 2024;66:546–78.
86. Zhang J, Nielsen R, Yang Z. Evaluation of an improved branch site likelihood method for detecting positive selection at the molecular level. Mol Biol Evol. 2005;22:2472–9.
87. Chen LY, Lu B, Morales-Briones DF, Moody ML, Liu F, Hu GW, et al. Phylogenomic analyses of Alismatales Shed Light into adaptations to aquatic environments. Mol Biol Evol. 2022;39:msac079.
88. Madoka Y, Tomizawa KI, Mizoi J, Nishida I, Nagano Y, Sasaki Y. Chloroplast transformation with modified *accD* operon increases acetyl-CoA carboxylase and causes extension of leaf longevity and increase in seed yield in tobacco. Plant Cell Physiol. 2002;43:1518–25.
89. Rawsthorne S. Carbon flux and fatty acid synthesis in plants. Prog Lipid Res. 2002;41:182–96.
90. Kode V, Mudd EA, Iamtham S, Day A. The tobacco plastid *accD* gene is essential and is required for leaf development. Plant J. 2005;44:237–44.
91. Caroca R, Howell KA, Malinova I, Burgos A, Tiller N, Pellizzer T, et al. Knockdown of the plastid-encoded acetyl-CoA carboxylase gene uncovers functions in metabolism and development. Plant Physiol. 2021;185:1091–110.
92. Pu FD, Watson MF. Oenanthe Linnaeus. In: Wu ZY, Raven PH, editors. Flora of China V.14. Beijing and St. Louis: Science Press and Missouri Botanical Garden Press; 2005. p. 130–2.
93. Pu FD, Watson MF. Sium Linnaeus. In: Wu ZY, Raven PH, editors. Flora of China V.14. Beijing and St. Louis: Science Press and Missouri Botanical Garden; 2005. p. 115–6.
94. Pan ZH, Watson MF. Cryptotaenia de Candolle. In: Wu ZY, Raven PH, editors. Flora of China V.14. Beijing and St. Louis: Science Press and Missouri Botanical Garden; 2005. p. 80.
95. Sheh ML, Watson MF. Cicuta Linnaeus. In: Wu ZY, Raven PH, editors. Flora of China V.14. Beijing and St. Louis: Science Press and Missouri Botanical Garden Press; 2005. p. 77.
96. Fleischmann TT, Scharff LB, Alkatib S, Hasdorf S, Schottler MA, Bock R. Nonessential plastid-encoded ribosomal proteins in tobacco: a developmental role for plastid translation and implications for reductive genome evolution. Plant Cell. 2011;23:3137–55.
97. Schippers JHM, Mueller-Roeber B. Ribosomal composition and control of leaf development. Plant Sci. 2010;179:307–15.
98. Tiller N, Weingartner M, Thiele W, Maximova E, Schottler MA, Bock R. The plastid-specific ribosomal proteins of Arabidopsis thaliana can be divided into non-essential proteins and genuine ribosomal proteins. Plant J. 2012;69:302–16.
99. Robles P, Quesada V. Unveiling the functions of plastid ribosomal proteins in plant development and abiotic stress tolerance. Plant Physiol Bioch. 2022;189:35–45.
100. Wicke S, Schneeweiss GM, depamphilis CW, Müller KF, Quandt D. The evolution of the plastid chromosome in land plants: gene content, gene order, gene function. Plant Mol Biol. 2011;76:273–97.
101. Wilson RH, Hayer-Hartl M. Complex chaperone dependence of Rubisco biogenesis. Biochemistry. 2018;57:3210–6.
102. Whitney SM, Sharwood RE. Rubisco engineering by plastid transformation and protocols for assessing expression. Methods Mol Biol. 2021;2317:195–214.
103. Kapralov MV, Filatov DA. Widespread positive selection in the photosynthetic rubisco enzyme. BMC Evol Biol. 2007;7: 73.
104. Iida S, Miyagi A, Aoki S, Ito M, Kadono Y, Kosuge K. Molecular adaptation of *rbcL* in the heterophyllous aquatic plant Potamogeton. PLoS ONE. 2009;4:e4633.
105. Rumeau D, Peltier G, Cournac L. Chlororespiration and cyclic electron flow around PSI during photosynthesis and plant stress response. Plant Cell Environ. 2007;30:1041–51.
106. Yamori W, Sakata N, Suzuki Y, Shikanai T, Makino A. Cyclic electron flow around photosystem I via chloroplast NAD(P)H dehydrogenase (NDH) complex performs a significant physiological role during photosynthesis and plant growth at low temperature in rice. Plant J. 2011;68:966–76.
107. Suorsa M, Sirpiö S, Aro EM. Towards characterization of the chloroplast NAD(P)H dehydrogenase complex. Mol Plant. 2009;2:1127–40.
108. Martin M, Sabater B. Plastid *ndh* genes in plant evolution. Plant Physiol Bioch. 2010;48:636–45.
109. Xie DF, Xie C, Ren T, Song BN, Zhou SD, He XJ. Plastid phylogenomic insights into relationships, divergence, and evolution of Apiales. Planta. 2022;256:117.
110. Drescher A, Ruf S, Calsa TJr, Carrer H, Bock R. The two largest chloroplast genome-encoded open reading frames of higher plants are essential genes. Plant J. 2000;22:97–104.
111. Kikuchi S, Asakura Y, Imai M, Nakahira Y, Kotani Y, Hashiguchi Y, et al. A Ycf2- FtsHi heteromeric AAA-ATPase complex is required for chloroplast protein import. Plant Cell. 2018;30:2677–703.
112. Nakai M. YCF1: a green TIC: response to the De Vries et al commentary. Plant Cell. 2015;27:1834–8.

Publisher's Note